# The nano-scale molecule with the longest delocalized metal–metal bonds: linear heptacobalt(II) metal string complexes $[Co_7(\mu_7\text{-}L)_4X_2]$†‡

**Wen-Zhen Wang,[a,b] Rayyat Huseyn Ismayilov,[a,b] Gene-Hsiang Lee,[a] Isiah Po-Chun Liu,[a,b] Chen-Yu Yeh[c] and Shie-Ming Peng*[a,b]**

***Received 5th October 2006, Accepted 11th December 2006***
***First published as an Advance Article on the web 9th January 2007***
**DOI: 10.1039/b614661a**

A new type of pyrazine-modulated oligo-α-pyridylamino ligands, $N^2$-(pyrazin-2-yl)-$N^6$-(6-(pyrazin-2-ylamino)pyridin-2-yl)pyridine-2,6-diamine ($H_3$pzpz) (**1**) and $N^2$-(pyrazin-2-yl)-$N^6$-(6-(pyridin-2-ylamino)pyridin-2-yl)pyridine-2,6-diamine ($H_3$tpz) (**2**), were synthesized and characterized by IR, $^1$H NMR and MS(FAB). Using **1** and **2**, the linear heptacobalt(II) metal string complexes $[Co_7(\mu_7\text{-}L)_4X_2]$ (L = $pzpz^{3-}$, X = $Cl^-$ (**3**), $NCS^-$ (**4**); L = $tpz^{3-}$, X = $Cl^-$ (**5**), X = $NCS^-$ (**6**)) were synthesized and structurally characterized. The structures showed the shortest Co–Co distance (2.194 Å) and the longest Co chain (13.5 Å) obtained to date with direct Co–Co bonds. The Co–Co distances are in the range 2.194–2.309 Å. Electrochemical studies showed two reversible oxidations and one reversible reduction, while all the redox reactions of $H_3$pzpz complexes, **3** and **4**, occurred at higher potentials than $H_3$tpz complexes, **5** and **6**. The complexes **3–6** are fairly stable to oxidation. Temperature-dependent magnetic research on **3–6** revealed anomalous magnetic behavior with intermediate magnetic moment values between quartet and doublet states, and deviation from the Curie–Weiss law.

## Introduction

In the past decade, increasing attention has been given to extended metal atom chains (EMAC) due to their importance in the fundamental understanding of metal–metal interactions and in potential applications such as molecular metal wires and switches.[1] A series of tri-,[2] tetra-,[3] penta-,[4] hexa-,[5] hepta-,[6] and nona-[7] nuclear metal string complexes have been synthesized by employing oligo-α-pyridylamino ligands (Scheme 1). The typical structure of this family includes a linear metal chain helically wrapped by four deprotonated oligo-α-pyridylamido ligands, with all the pyridine nitrogen atoms and amido nitrogen atoms coordinated in a *syn* form. The adjacent pyridyl rings of the ligands are not coplanar due to the repulsion of the β-H atoms, and the dihedral angle between them is about 45°. Hence the twisted, wrapping ligand will fulfill a single term around the metal array line when it contains nine pyridyl rings (thus the metal string complex consists of seventeen metal atoms), and the molecule theoretically can be extended to infinite one-dimension. For this purpose the synthesis of longer EMAC than currently produced is one of our research targets. However, synthetic difficulty increases and yields decrease with an increase in the number of metal atoms in EMAC. The longest structurally characterized EMAC molecules obtained up to now contain nine metal atoms for nickel[7a] and chromium,[7b] and five for cobalt[4a–c] and ruthenium[8] complexes. Previous research has revealed that in nickel string compounds both terminal nickel atoms exist in high spin states whereas all the inner nickel atoms exhibit low spin states and no nickel–nickel bonds were observed between nickel atoms. Cobalt and chromium string complexes, however, showed significant metal–metal interaction and higher electronic conductivity than those of nickel strings.[1] The syntheses of EMAC with metal–metal bonds are especially difficult in spite of the fact that they are more important in function as molecular electronic devices, for the electron delocalization among metal chain through metal–metal bonds are crucial for electron conductivity. Using our standard synthetic method for EMAC (naphthalene as solvent and potassium butoxide as base), the yield of $[Ni_3(dpa)_4Cl_2]$ (Hdpa = di(2-pyridyl)amine) reached near 90%, $[Cr_3(dpa)_4Cl_2]$ more than 70%, but the yield of $[Co_3(dpa)_4Cl_2]$ was around 40%. We synthesized $[Co_5(tpda)_4Cl_2]$ ($H_2$tpda = tripyridyldiamine) nine years ago with a yield of 5%,[4b] but many efforts to synthesize longer cobalt EMAC were not successful. Recently we developed a new type of ligand, pyrazine-modulated oligo-α-pyridylamine by including pyrazine instead of pyridine ring(s) in oligo-α-pyridylamino ligands (Scheme 2).[7b,9] The introduction of nitrogen-rich aromatic pyrazine rings to the ligand significantly improves the reactivity, resulting in very pure target compounds. From this strategy we successfully obtained a linear heptanuclear cobalt complex, which is the longest metal string molecule for a cobalt complex thus far obtained. Here we report

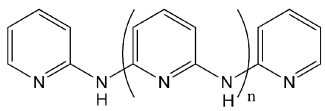

**Scheme 1**

[a]*Department of Chemistry, National Taiwan University, Taipei, Taiwan, ROC*
[b]*Institute of Chemistry, Academia Sinica, Taipei, Taiwan, ROC. E-mail: smpeng@ntu.edu.tw*
[c]*Department of Chemistry, National Chung Hsing University, Taichung, Taiwan, ROC*

† The HTML version of this article has been enhanced with colour images.
‡ Electronic supplementary information (ESI) available: Fig. S1 and S2. See DOI: 10.1039/b614661a

 


**Scheme 2**

two new pyrazine-modulated ligands, $N^2$-(pyrazin-2-yl)-$N^6$-(6-(pyrazin-2-ylamino)pyridin-2-yl)pyridine-2,6-diamine ($H_3$pzpz) (**1**) and $N^2$-(pyrazin-2-yl)-$N^6$-(6-(pyridin-2-ylamino)pyridin-2-yl)pyridine-2,6-diamine ($H_3$tpz) (**2**), and their heptanuclear cobalt complexes $[Co_7(\mu_7\text{-pzpz})_4Cl_2]$ (**3**), $[Co_7(\mu_7\text{-pzpz})_4(NCS)_2]$ (**4**), $[Co_7(\mu_7\text{-tpz})_4Cl_2]$ (**5**) and $[Co_7(\mu_7\text{-tpz})_4(NCS)_2]$ (**6**).

## Results and discussion

### Syntheses and structures

The ligands $H_3$pzpz **1** and $H_3$tpz **2** were synthesized by palladium-catalyzed cross-coupling of aromatic amine and halogenide, in the presence of catalysts [$Pd_2(dba)_3$, BINAP, Bu$^t$ONa] in refluxing benzene under argon (Scheme 3), and characterized by IR, $^1$H NMR and MS(FAB).

The $[Co_7(\mu_7\text{-pzpz})_4Cl_2]$ (**3**) and $[Co_7(\mu_7\text{-tpz})_4Cl_2]$ (**5**) complexes were synthesized by reacting anhydrous $CoCl_2$ with corresponding ligands in an argon atmosphere using naphthalene as solvent and Bu$^t$OK as base to deprotonate the amine group. The yield was low, but careful separation after the reaction produced a very pure target product, which afforded us the succeeding measurement. Thiocyanate complexes $[Co_7(\mu_7\text{-pzpz})_4(NCS)_2]$ (**4**) and $[Co_7(\mu_7\text{-tpz})_4(NCS)_2]$ (**6**) were obtained by axial ligand exchanging reactions from **3** and **5**, respectively. All the heptacobalt complexes **3–6** showed considerable solubility in common organic solvents, such as $CH_2Cl_2$, chloroform, benzene, methanol, acetone *etc.* The crystal data of **3–6** are listed in Table 1 and structures shown in Fig. 1, Fig. 1S,‡ Fig. 2S‡ and Fig. 2, respectively. There are two chemically equivalent units in complex **6**. As in other oligo-α-pyridylamino metal string complexes, the seven Co(II) ions are collinear with the Co–Co–Co angles in the range 177.4–179.9°, and the heptacobalt chain is helically wrapped by four deprotonated ligands, all-*syn* coordinated. The whole length of the $Co_7$ chain is about 13.5 Å. The molecule lengths of chloride complexes (**3** and **5**) and thiocyanate complexes (**4** and **6**) are 18.3 and 23.4 Å, respectively. In **3** and **5**, the molecular structures are disordered because they contain both left-turn and right-turn helical forms of

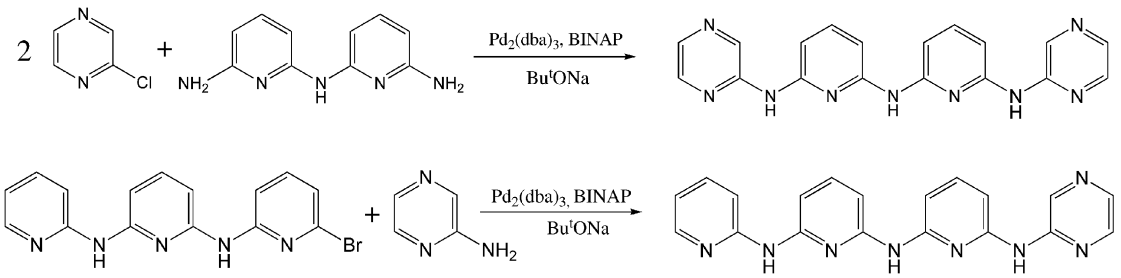


**Scheme 3**

**Table 1** Crystal data for **3–6**

| Compound | **3**·1.5$C_2H_5OC_2H_5$ | **4**·4$C_6H_{14}$·$H_2O$ | **5**·$C_2H_5OC_2H_5$ | **6**·$C_2H_5OC_2H_5$·0.5$CH_2Cl_2$ |
|---|---|---|---|---|
| Formula | $C_{78}H_{63}Cl_2Co_7N_{36}O_{1.5}$ | $C_{98}H_{106}Co_7N_{38}OS_2$ | $C_{80}H_{62}Cl_2Co_7N_{32}O$ | $C_{82.5}H_{63}ClCo_7N_{34}OS_2$ |
| Formula weight | 2012.05 | 2308.84 | 1971.03 | 2058.75 |
| Crystal system | Orthorhombic | Monoclinic | Monoclinic | Monoclinic |
| Space group | $P2_12_12$ | $C2/c$ | $P2/c$ | $C2/c$ |
| $a$/Å | 32.9247(13) | 30.6410(10) | 13.5397(2) | 27.7926(8) |
| $b$/Å | 12.8185(5) | 16.2874(6) | 10.3523(2) | 20.7712(5) |
| $c$/Å | 10.2151(4) | 22.2876(7) | 28.4128(5) | 30.0433(7) |
| $\beta$/° | 90 | 109.727(2) | 91.7760(9) | 95.0229(10) |
| Volume/Å$^3$, $Z$ | 4311.2(3), 2 | 10470.1(6), 4 | 3980.62(12), 2 | 17277.0(8), 8 |
| $D_c$/Mg m$^{-3}$ | 1.550 | 1.465 | 1.644 | 1.583 |
| Absorption coefficient/mm$^{-1}$ | 1.444 | 1.188 | 1.560 | 1.459 |
| Crystal size/mm | 0.25 × 0.15 × 0.03 | 0.27 × 0.10 × 0.04 | 0.25 × 0.20 × 0.10 | 0.35 × 0.15 × 0.15 |
| $\theta$ range for data collection/° | 1.24–25.00 | 1.41–25.00 | 1.43–25.00 | 1.23–25.00 |
| Reflection collected | 26661 | 28398 | 47630 | 67405 |
| Independent reflections | 7561 ($R_{int}$ = 0.0623) | 9230 ($R_{int}$ = 0.0980) | 7003 ($R_{int}$ = 0.0763) | 15219 ($R_{int}$ = 0.0846) |
| $R_1$, $Rw_2$ [$I > 2\sigma(I)$] | 0.0826, 0.2260 | 0.0881, 0.2592 | 0.0787, 0.2672 | 0.0899, 0.2705 |
| $R_1$, $Rw_2$ (all data) | 0.1494, 0.2818 | 0.2063, 0.3302 | 0.1417, 0.3174 | 0.1910, 0.3299 |
| GOF | 1.024 | 1.061 | 1.095 | 1.118 |

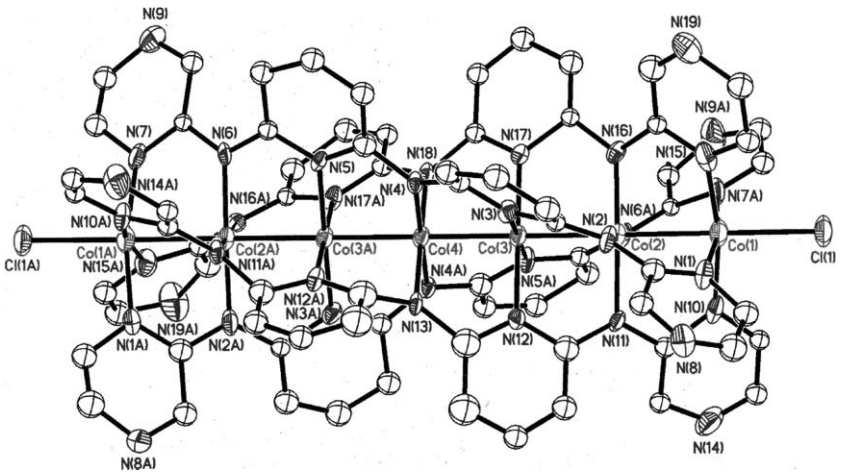


**Fig. 1** The crystal structure of $[Co_7(\mu_7\text{-pzpz})_4Cl_2]$ (**3**). Atoms are drawn at the 50% probability level. Disordered atomic positions and hydrogen atoms are omitted for clarity. Label A was generated through the symmetry operation $(-x, -y, z)$.

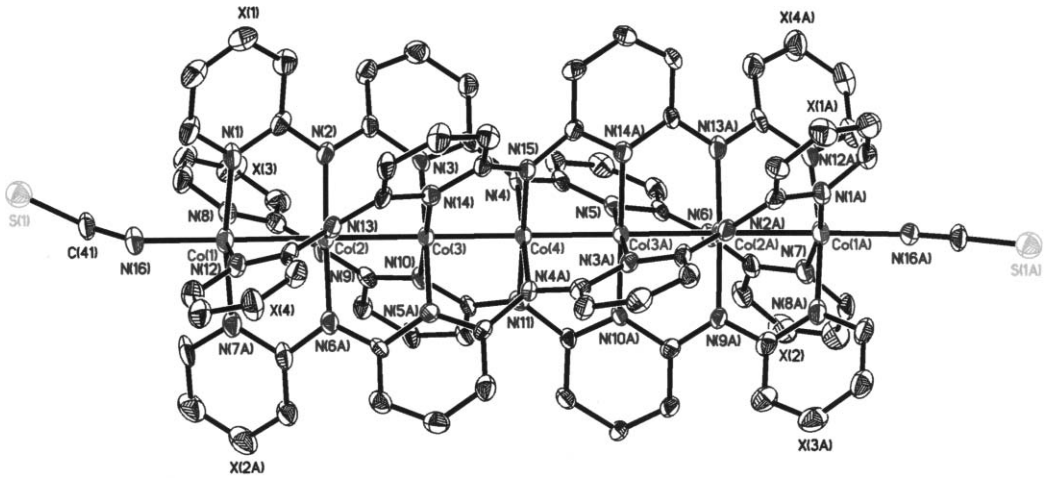


**Fig. 2** The crystal structure of $[Co_7(\mu_7\text{-tpz})_4(NCS)_2]$ (**6**). Atoms are drawn at the 50% probability level. Disordered atomic positions and hydrogen atoms are omitted for clarity. Label A was generated through the symmetry operation $(1 - x, y, 1/2 - z)$.

ligands. The molecule of **3–6** resides on a crystallographic site of 2-fold symmetry with the central cobalt atom on a 2-fold axis perpendicular to the molecular chain. In the thiocyanate complexes **4** and **6**, the central cobalt atom is at the symmetrical center, and the structure of $NCS^-$ anions are disordered, whereas bridging ligands are not disordered. For $H_3$tpz complexes **5** and **6**, the probability of pyrazine or pyridine for every terminal aromatic ring is 50%, actually owing to the technical limit to discriminate between nitrogen and carbon atoms. [Fig. 1 and Fig. 2 are the structures of $[Co_7(\mu_7\text{-pzpz})_4C_{12}]$ (**3**) and $[Co_7(\mu_7\text{-tpz})_4(NCS)_2]$ (**6**), repectively.]

Selected bond lengths and angles of complexes **3–6** are listed in Table 2, and a comparison of Co–Co distances and Co–N distances among the tri-, penta- and heptacobalt(II) complexes is shown in Scheme 4. The Co–Cl distances in **3** and **5** (2.373(3) and 2.374(2) Å, respectively) are short in comparison with $[Co_3(\mu_3\text{-dpa})_4Cl_2]$ (average 2.396(4) Å[2a]) and $[Co_5(\mu_5\text{-tpda})_4Cl_2]$ (2.445(2) Å), and the Co–N(NCS) distances in **4** and **6** (2.032(7) and 2.040(8) Å, respectively) are shorter than the respective bonds in $[Co_5(\mu_5\text{-tpda})_4(NCS)_2]$ (average 2.065(1) Å). Three different Co–Co distances were observed for every heptacobalt complex: the longest one for the terminal Co–Co bonds (Co(1)–Co(2)), a medium distance between the intermediate Co(2)–Co(3) bonds, and the shortest between the innermost Co–Co bonds (Co(3)–Co(4)). Decreases in metal–metal distances from the terminal to the centre of molecules have been observed for both nickel and cobalt EMACs.[7a] It is noticeable that Co(3)–Co(4) distances, which ranged from 2.194 to 2.199 Å in EMACs **3–6**, are the shortest Co–Co bonds in all cobalt EMACs thus far obtained, and the lengths are indicative of obvious metal–metal bonds between the cobalt atoms. The Co(1)–Co(2) distances in chloride complexes **3** and **5** are longer than those in thiocyanate complexes **4** and **6**, as well as in the pentacobalt EMAC $[Co_5(\mu_5\text{-tpda})_4Cl_2]$ and $[Co_5(\mu_5\text{-tpda})_4(NCS)_2]$. In **3–6**, ligands $H_3$pzpz **1** and $H_3$tpz **2** were both deprotonated and three negatively charged. The charge distributions and π bond orders of ligand anions, $pzpz^{3-}$ and $tpz^{3-}$, were calculated based on resonance analysis and are shown in Scheme 5. The negative charges were restrained to resonance only on the coordinated nitrogen atoms for simplification. As seen from Scheme 5, since the negative density on amido nitrogen atoms (N(2) and N(4)) are higher than that on pyridyl nitrogen

 

**Table 2** Selected bond distances (Å) and angles (°) for **3–6**

| Complex | **3** | **4** | **5** | **6**[e] |
|---|---|---|---|---|
| Co(1)–Co(2) | 2.300(2) | 2.286(2) | 2.309(1) | 2.276(2) |
| Co(2)–Co(3) | 2.260(2) | 2.261(2) | 2.258(1) | 2.252(2) |
| Co(3)–Co(4) | 2.199(1) | 2.196(1) | 2.196(1) | 2.194(1) |
| Co(1)–N(1)[a] | 1.958(12) | 1.962(8) | 2.003(7) | 1.975(8) |
| Co(2)–N(2)[a] | 1.927(20) | 1.911(8) | 1.908(12) | 1.908(8) |
| Co(3)–N(3)[a] | 1.946(9) | 1.939(7) | 1.929(6) | 1.936(7) |
| Co(4)–N(4)[a] | 1.916(20) | 1.928(7) | 1.914(17) | 1.913(9) |
| Co(1)–X[b] | 2.373(3) | 2.032(7) | 2.374(2) | 2.040(8) |
| N(1)–C(1)[a] | 1.350(30) | 1.362(12) | 1.338(17) | 1.354(12) |
| N(1)–C(4)[a] | 1.400(30) | 1.372(12) | 1.391(16) | 1.360(11) |
| N(2)–C(4)[a] | 1.356(30) | 1.372(11) | 1.372(19) | 1.366(11) |
| N(2)–C(5)[a] | 1.374(30) | 1.376(11) | 1.388(19) | 1.382(11) |
| N(3)–C(5)[a] | 1.364(30) | 1.368(10) | 1.362(18) | 1.365(11) |
| N(3)–C(9)[a] | 1.362(30) | 1.360(10) | 1.373(15) | 1.368(11) |
| N(4)–C(9)[a] | 1.406(30) | 1.370(10) | 1.393(17) | 1.380(11) |
| X(1)[c]–C(2)[a] | 1.361(40) | 1.365(14) | 1.348(20) | 1.368(15) |
| X(1)[c]–C(3)[a] | 1.395(30) | 1.306(12) | 1.400(19) | 1.347(13) |
| C(1)–C(2)[a] | 1.301(40) | 1.343(15) | 1.372(30) | 1.363(15) |
| C(3)–C(4)[a] | 1.446(40) | 1.401(14) | 1.386(20) | 1.398(13) |
| C(5)–C(6)[a] | 1.360(40) | 1.391(13) | 1.366(20) | 1.384(12) |
| C(6)–C(7)[a] | 1.396(40) | 1.391(13) | 1.366(20) | 1.373(13) |
| C(7)–C(8)[a] | 1.410(40) | 1.388(13) | 1.405(17) | 1.382(13) |
| C(8)–C(9)[a] | 1.406(30) | 1.383(12) | 1.384(20) | 1.398(12) |
| X[b]–Co(1)–Co(2) | 179.75(15) | 179.4(2) | 179.52(8) | 179.1(2) |
| Co(1)–Co(2)–Co(3) | 179.35(9) | 177.41(7) | 179.63(6) | 179.44(8) |
| Co(2)–Co(3)–Co(4) | 179.81(10) | 179.29(8) | 179.95(7) | 179.80(8) |
| Co(3)–Co(4)–Co(3A)[d] | 179.65(13) | 179.02(11) | 179.62(8) | 179.94(10) |
| Molecule length/Å | 18.27 | 23.40 | 18.27 | 23.12 |

[a] Average value from the four wrapping ligands. [b] X = Cl for **3** and **5**, X = N from $NCS^-$ for **4** and **6**. [c] X(1) = N for **3** and **4**, X(1) = N or C for **5** and **6**. [d] Symmetry codes for **3**, A = $-x$, $-y$, $z$; for **4**, A = $-x-1$, $y$, $-z+1/2$; for **5**, A = $-x$, $y$, $-z+1/2$; for **6**, A = $-x+1$, $y$, $-z+1/2$ (unit 1) and A = $-x$, $y$, $-z+1/2$ (unit 2). [e] Average value from the two molecules.

atoms (N(1) and N(3)), thus the $Co–N_{amido}$ bonds (Co(2)–N(2) and Co(4)–N(4)) are stronger than $Co–N_{pyridyl}$ bonds (Co(1)–N(1) and Co(3)–N(3)), and consequently the $Co–N_{amido}$ bond distances are shorter. The least negatively charged nitrogen atom is the terminal one, and the terminal Co(1)–N bond lengths are longest. It is noticeable that Co(1)–N bond lengths of **3** and **4** (1.958(12) and 1.962(8) Å, respectively) are both shorter than those of **5** and **6** (2.003(7) and 1.975(8) Å, respectively), consistent with the two-pyrazine-containing ligand $H_3$pzpz providing a stronger ligand field than the one-pyrazine-containing ligand $H_3$tpz. Among all C–C bonds, the π bond order on C(1)–C(2), 71/112, is the highest, and the C(1)–C(2) bond distance is the shortest, indicating the strongest π bond character between C(1)–C(2). In the same case, N(2)–C(5) and N(4)–C(9) have the lowest π bond order among all N–C bonds, and their distances are comparably longer (Table 2).

## Electrochemisrty

The redox properties of EMACs are pivotal for their function as molecular devices. The loss and gain of electrons provide bistable states, which are the base of molecular switches, and the electronic transfer (electron flow) through the molecules endues them with electron conductivity as molecular wires. Therefore, it is essential to study the electrochemical properties of these

**Table 3** Redox potentials for complexes **3–6**

| Complex | **3** | **4** | **5** | **6** |
|---|---|---|---|---|
| $E_{1/2}$ (Ox2)/V | 0.882 | 0.932 | 0.700 | 0.764 |
| $E_{1/2}$ (Ox1)/V | 0.622 | 0.676 | 0.402 | 0.461 |
| $E_{1/2}$ (Red)/V | −0.119 | −0.080 | −0.300 | −0.273 |

heptacobalt complexes. The cyclic voltammograms show that all these complexes exhibit three reversible one-electron redox couples and the electrochemical data are summarized in Table 3. As an example, the cyclic voltammogram of complex **3** in $CH_2Cl_2$ shows three redox couples at $E_{1/2}$ = −0.12, +0.62, and +0.88 V (Fig. 3). The redox potentials of the dithiocyanate analogue **4** exhibit slightly anodic shifts, as found for $[Ni_3(\mu_3\text{-}L)_4X_2]$ (HL = di(2-pyrazyl)amine (Hdpza), di(2-pyridyl)amine (Hdpa); X = $Cl^-$, $NCS^-$) and other polynuclear EMAC.[10,11] For the complexes **5** and **6**, in which the $Co_7$ core is supported by four one-pyrazine-modulated ligands, the redox potentials are cathodically shifted as compared to those of two-pyrazine-modulated complexes **3** and

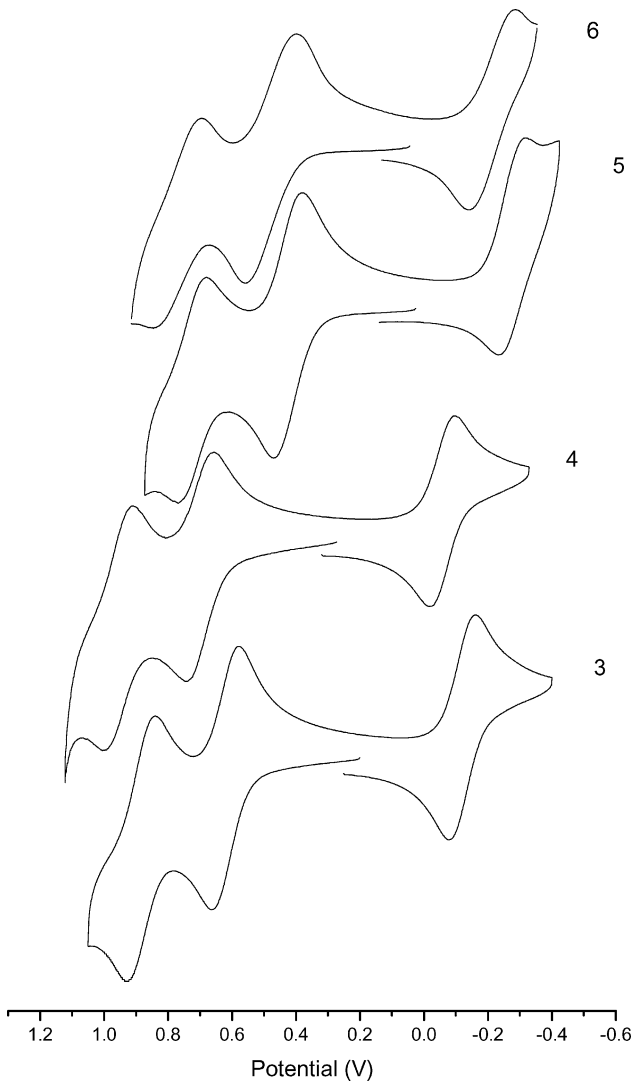


**Fig. 3** Cyclic voltammogramms of heptacobalt(II) EMAC **3–6** in $CH_2Cl_2$ containing 0.1 M TBAP.

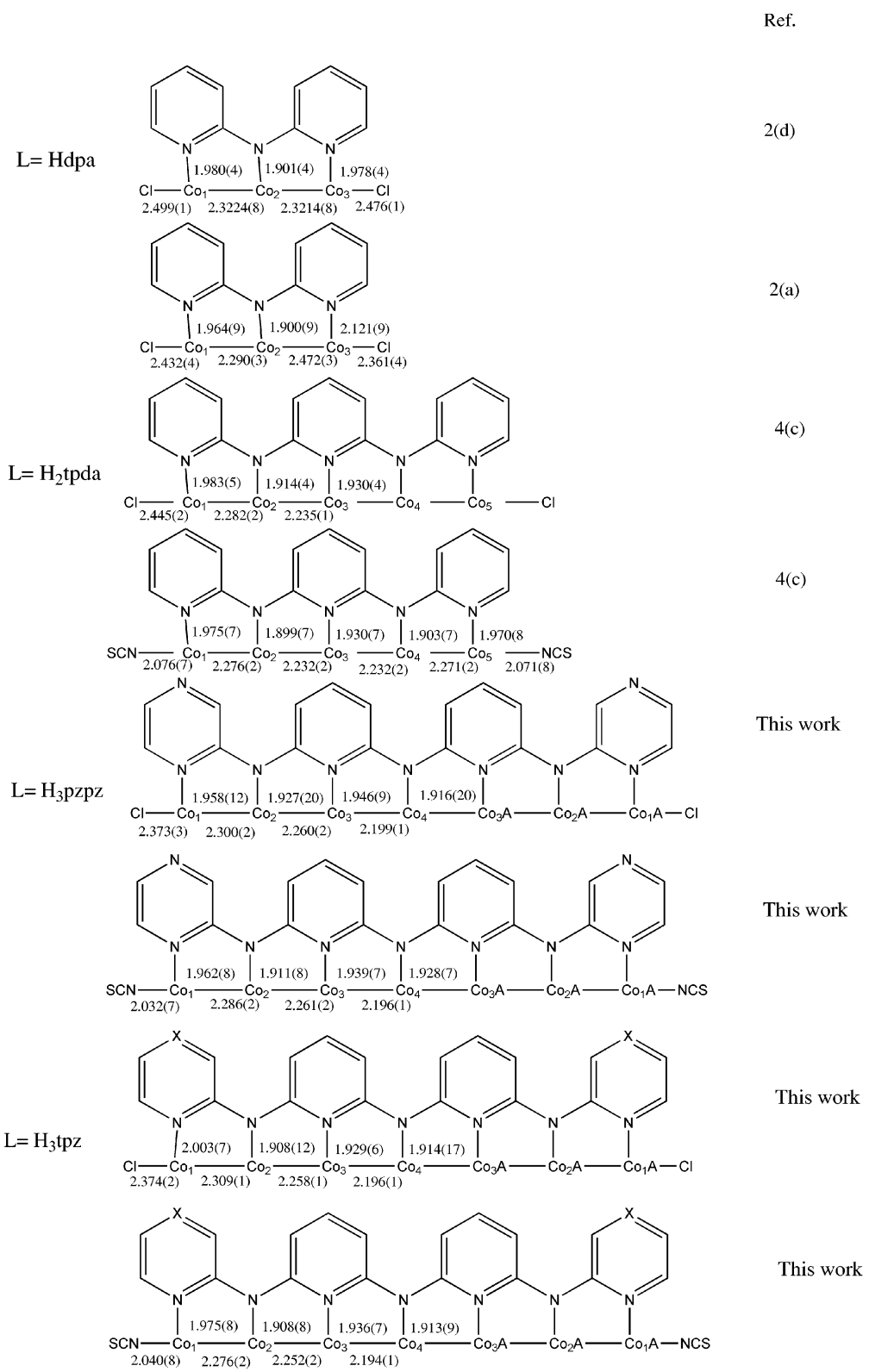


**Scheme 4** Comparison of bond distances in cobalt EMAC. The occupancy of X is 50% nitrogen and 50% carbon.

**4**. This may be attributed to the electron-withdrawing effect of the pyrazine ring, and is consistent with our previous research on trinickel EMAC: The complex $[Ni_3(\mu_3\text{-dpza})_4X_2]$ (Hdpza = di(2-pyrazyl)amine, X = $Cl^-$, $NCS^-$) is more resistant to oxidation whereas susceptible to reduction compared with pyridyl complexes $[Ni_3(\mu_3\text{-dpa})_4X_2]$.[10] Thus, introduction of electron-withdrawing group pyrazine to the supporting ligand facilitates reduction and retards oxidation of the $Co_7$ chain.

 

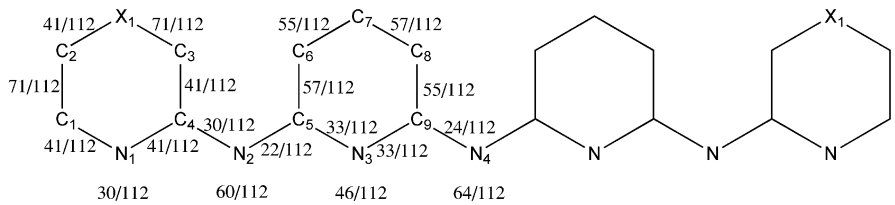


**Scheme 5** Negative charge distribution and π bond orders of ligand anions, $pzpz^{3-}$ and $tpz^{3-}$. X(1) = N in **3** and **4**. For **5** and **6**, the occupancy of X(1) is 50% for nitrogen and 50% carbon.

It is impossible to determine the oxidation states of the complexes at a certain potential simply by judging from the cyclic voltammograms. For example, the electrochemical process at $E_{1/2} = -0.12$ V for **3** could correspond to **3**/**3**$^{+}$ or **3**$^{-}$/**3**. To determine the oxidation states, spectroelectrochemical techniques were employed (Fig. 4 and 5). Fig. 5 shows the spectral changes of **3** at various applied potentials from 0.00 to −0.25 V. The peaks at 275, 590, and 645 nm decrease, and those at 310, 380, 715, and 1005 nm increase as the applied potential increases. The absorption spectrum was restored when the applied potential of −0.25 V was set back to 0.00 V. This indicates that the electrochemical process is reversible and the wave at $E_{1/2} = -0.12$ V corresponds to the reduction of **3** to form **3**$^{-}$. The band at 1005 nm in the near IR region can be ascribed to the intervalence charge transfer of reductive product $Co_7^{13+}$. The clear isosbestic points at 310, 345, 535, 690 and 1150 nm indicate that no intermediates were produced during the reduction process. The first and second oxidation of **3** in $CH_2Cl_2$ containing 0.1 M TBAP were also performed at various applied potentials from +0.40 to +0.95 V. The absorption bands at 280, 380, 595 and 645 nm decrease, and those at 740 nm and near IR increase with isosbestic points at 670 and 1195 nm as the applied potential increases from +0.40 to +0.66 V. Further oxidation at $E_{appl.} = +0.95$ V results in a further increase in the absorption intensity of the near IR band, which corresponds to the intervalence charge transfer of mixed-valence species $Co_7^{16+}$.

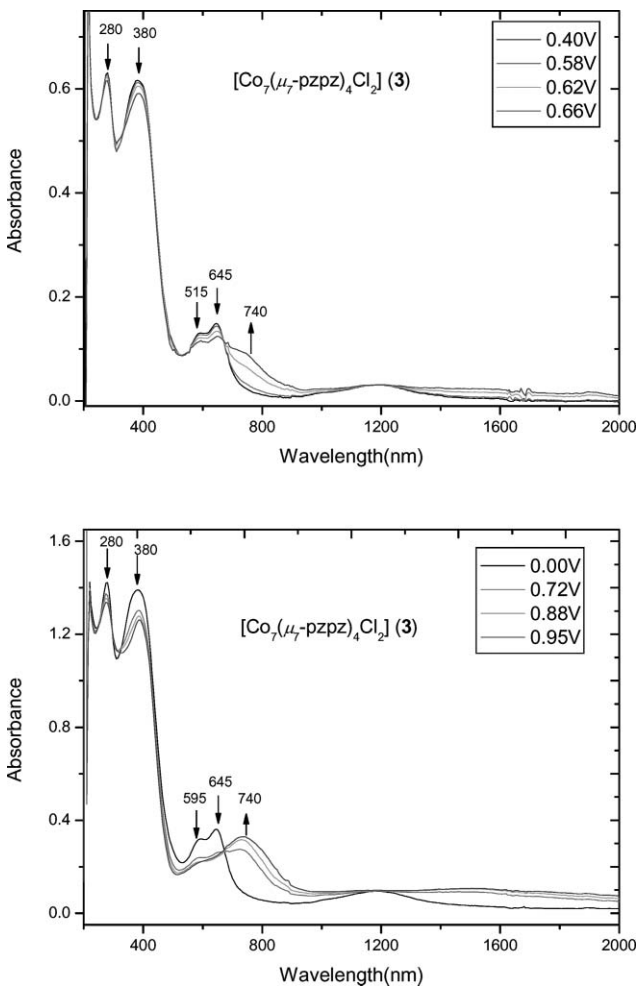


**Fig. 4** Spectral changes for first oxidation (a) and for second oxidation (b) of $[Co_7(\mu_7\text{-pzpz})_4Cl_2]$ (**3**) in $CH_2Cl_2$ with 0.1 M TBAP at various applied potentials from 0.40 to 0.66 V and from 0.72 to 0.95 V, respectively.

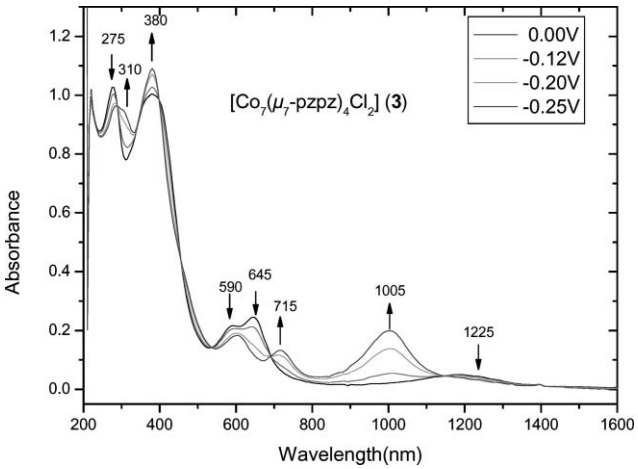


**Fig. 5** Spectral changes for reduction of $[Co_7(\mu_7\text{-pzpz})_4Cl_2]$ (**3**) in $CH_2Cl_2$ with 0.1 M TBAP at various applied potentials from 0.00 to −0.25 V.

## Magnetic properties

The effective magnetic moments of complexes **3**, **5** and **6** are depicted as a function of temperature in Fig. 6, and results of **3–6** are listed in Table 4. The magnetic behavior is similar for all complexes **3–6**. The $\mu_{eff}$ values at room temperature lay in the range 2.70–3.87 $\mu_B$, and decreased slightly upon cooling, reaching 2.12–2.89 $\mu_B$ at 2 K. The complexes **3–6** exhibited obvious deviation from Curie behavior whereas there was no evidence of spin crossover clearly observed as was the case for tricobalt(II) EMAC.[2a,2d,12] Analysis on the magnetic moment values of **3–6** at room temperature revealed the following important points: (1) The $\mu_{eff}$ of complexes of two-pyrazine-modulated ligand ($H_3pzpz$), **3** and **4** (2.70 and 2.95 $\mu_B$, respectively), are much lower than

**Table 4** Magnetic data for **3–6**

| Complex | **3** | **4** | **5** | **6** |
|---|---|---|---|---|
| $\mu_{eff}$ at 300 K/$\mu_B$ | 2.70 | 2.95 | 3.87 | 3.51 |
| $\mu_{eff}$ at 2 K/$\mu_B$ | 2.12 | 2.61[a] | 2.89 | 2.46 |
| Co(1)–N/Å | 1.958(1) | 1.964(8) | 1.999(7) | 1.976(8) |

[a] Data measured at 5 K.

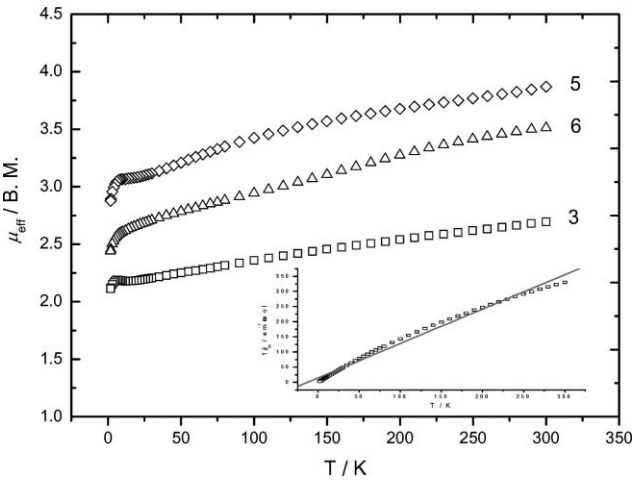


**Fig. 6** Experimental $\mu_{eff}$ values in dependence on temperature from susceptibility data for complexes **3** (□), **5**(◇) and **6**(△). Inset: Reciprocal dependence of the magnetic susceptibility on temperature. The solid lines result from least-square fits of the Curie Law.

those of one-pyrazine-modulated ligand ($H_3$tpz), **5** and **6** (3.87 and 3.51 $\mu_B$, respectively). The former are significantly higher than the theoretical spin-only value for a doublet ground state (1.73 $\mu_B$) but much lower than a quartet ground state (3.87 $\mu_B$), and the latter are very close to a spin-only value of the quartet ground state from three unpaired electrons. Considering that a two-pyrazine-containing ligand $H_3$pzpz provided a stronger ligand field than a one-pyrazine-containing ligand $H_3$tpz, this suggests that the electron configuration of heptacobalt EMAC may be adjusted practically by the ligands. The stronger ligand favors a lower magnetic moment. (2) The magnetic moment mostly depended on the terminal cobalt atoms. Comparison of the magnetic moments of **3–6** showed that the changes are exactly in accord with the change in Co(1)–N bond lengths: the longer the Co(1)–N bond length is, the higher the $\mu_{eff}$ value is (Table 4). (3) The bonding electron density is highly delocalized throughout the whole molecule. The paramagnetic density is actually very low as the molecules are fairly long, similar to that in pentacobalt EMAC.[4c] Based on previous research on EMAC, the magnetic interaction pathway is basically through the metal chain, this provided the evidence of formation of cobalt–cobalt bonds.[2f,13]

Anomalous magnetic behavior of octahedral cobalt(II) complexes had been observed for some time now with intermediate magnetic moment values between quartet and doublet states, and magnetic behavior deviation from the Curie–Weiss law.[14] Studies attributed this to a Boltzmann distribution over different spin states arising from spin–orbital coupling, and resulting in a doublet–quartet equilibrium. The magnetic moments of 2.12, 2.89 and 2.46 $\mu_B$ for complexes **3**, **5** and **6** at 2 K in this study, much higher values than a doublet ground state (1.73 $\mu_B$), suggesting a greater extent of orbital contribution. From MO theory, the larger a molecule is and the more metal atoms it contains, the lower energy gap between HOMO and LUMO. Consequently the higher spin state is more reachable. For heptanuclear Co(II) EMAC, the possible spin states span from $S = 1/2$ to $S = 7/2$, and the energy gaps are expected to be small. Thus spin equilibrium or a spin-admixed state is possibly existed. EPR spectra of **3** and **6** in $CH_2Cl_2$ glass showed a signal at $g = 5.65$, which also suggested the part distribution of higher spin state than $S = 1/2$.

### Molecular orbital calculation

In order to gain an insight into molecular orbitals for the heptacobalt(II) complexes, MO extended-Hückel calculations were performed on **3** and **4** by means of the CACAO program.[15a] The crystallographic coordinates were input as geometrical parameters and the *z*-axis was assumed as the X–Co7–X direction. The employed computational parameters were standard for the CACAO program. The resultant sequences of MOs are depicted in Fig. 7, in which the MOs closed to the Fermi level are similar for **3** and **4**. The HOMO is a δ-type orbital consisting of the $d_{xy}$ of seven cobalt atoms. Since the interaction between $d_{xy}$ orbitals is weak, the HOMO could be considered as localized MO.[15] Some σ-type orbitals with antibonding characters, 298a, 299a and 302a for

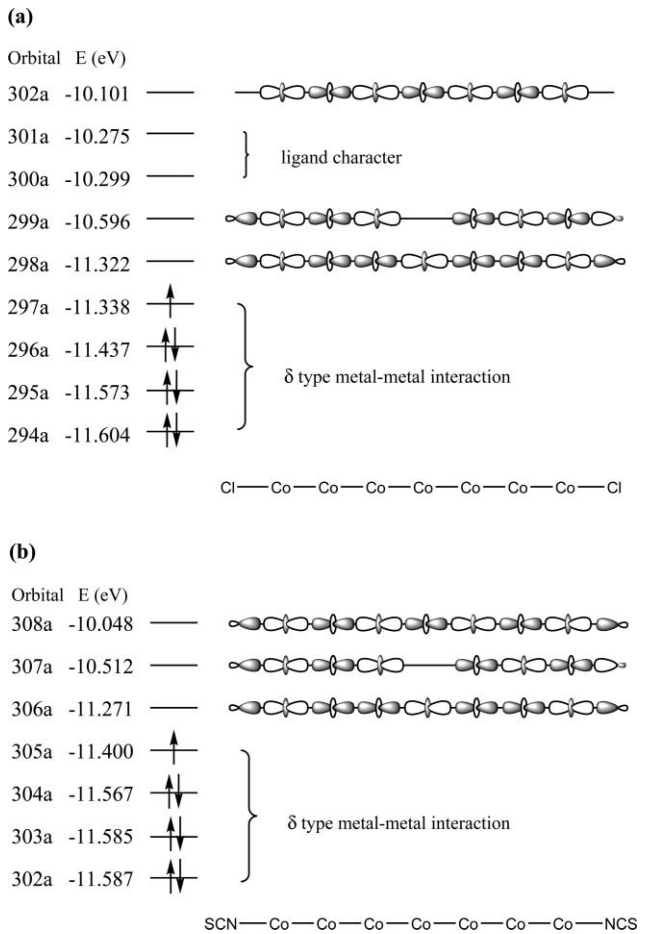


**Fig. 7** Sequence of the MOs for (a) **3** and (b) **4** obtained from extended-Hückel calculations. The electron distribution in HOMO of **3** is $(296a)^1$ $(297a)^1(298a)^1$ for the quartet state.

 

**3** and 306a, 307a and 308a for **4**, lie as LUMO in higher energy regions than in HOMO. These unoccupied σ* orbitals might imply that there exist σ-type metal–metal interactions within complexes as proposed in tri- and pentacobalt(II) EMAC.[4b,3g]

The significant difference between **3** and **4** is the HOMO–LUMO energy gap, which is 0.016 eV in the case of **3** and 0.129 eV for **4**, respectively. The former is much smaller than the latter. This could be due to an antibonding interaction between the σ* orbitals of the heptacobalt(II) centre and the axial ligands, which destabilize the σ* orbitals. Hence, the stronger NCS ligand increased the HOMO–LUMO energy gap. The small HOMO–LUMO energy gap in **3** indicates that an unpaired electron will hop from a localized orbital (297a) to a delocalized orbital (298a) at room temperature,[15c] and may play an important role in electron transfer when developing this type of complex as a nano-scale molecular wire. However, this phenomenon needs to be studied by high-level calculations and cannot be explained easily by means of the extended-Hückel level calculation.

## Conclusions

This work introduced the preparation of new types of pyrazine-modulated oligo-α-pyridylamino ligands, and their heptanuclear metal string cobalt(II) complexes, among the longest cobalt metal string complexes thus far developed. The heptacobalt metal string complex is collinear and contains intramolecular metal–metal bonds. Electrochemical studies showed two reversible oxidations and one reversible reduction, with redox reactions of $H_3$pzpz complexes occurring at higher potentials than for $H_3$tpz complexes. All the complexes **3–6** were stable to oxidation, whereas the $H_3$pzpz complexes easily underwent reduction. Magnetic research revealed that complexes **3–6** exhibited anomalous magnetic behavior, with intermediate magnetic moment values between quartet and doublet states, and deviation from the Curie–Weiss law.

## Experimental

### Materials

All reagents and solvents were obtained from commercial sources and were used without further purification unless otherwise noted. The $CH_2Cl_2$ was dried over $CaH_2$ and freshly distilled prior to use. Tetra-*n*-butylammonium perchlorate (TBAP) was recrystallized twice from ethyl acetate and dried under vacuum.

### Physical measurements

Absorption spectra were recorded on a HEWLETT PACKARD 8453 spectrophotometer. IR spectra were performed with a Perkin Elmer FT-IR Spectrometer PARAGON 1000 in the range of 400–4000 $cm^{-1}$. $^1H$ NMR was recorded in $(CD_3)_2SO$ and chemical shifts were reported in ppm relative to $(CD_3)_2SO$ ($\delta$ 2.49 ppm for $^1H$). FAB-MS mass spectra were obtained with a JEOL JMS-700 HF double focusing spectrometer operating in the positive ion detection mode. Molar magnetic susceptibility was recorded on a SQUID system with 2000 Gauss external magnetic field for complexes **3**, **5** and **6**, and 10 000 G for **4**. Electrochemistry was performed with a three-electrode potentiostat (CH Instruments, Model 750A) in $CH_2Cl_2$ deoxygenated by purging with prepurified nitrogen gas. Cyclic voltammetry was conducted with the use of a home-made three-electrode cell equipped with a BAS glassy carbon (0.07 $cm^2$) platinum (0.02 $cm^2$) disk as the working electrode, a platinum wire as the auxiliary electrode, and a home-made Ag/AgCl (saturated) reference electrode. The reference electrode is separated from the bulk solution by a double junction filled with electrolyte solution. Potentials are reported *vs.* Ag/AgCl (saturated) and referenced to the ferrocene/ferrocenium ($Fc/Fc^+$) couple which occurs at $E_{1/2} = +0.54$ V *vs.* Ag/AgCl (saturated). The working electrode was polished with 0.03 μm aluminium on Buehler felt pads and was put under ultrasonic radiation for 1 min prior to each experiment. The reproducibility of individual potential values was within ±5 mV. The spectroelectrochemical experiments were accomplished with the use of a 1 mm cuvette, a 100 mesh platinum gauze as working electrode, a platinum wire as the auxiliary electrode, and a Ag/AgCl (saturated) reference electrode.

### Preparation of compounds

***N*²-(pyrazin-2-yl)-*N*⁶-(6-(pyrazin-2-ylamino)pyridin-2-yl)pyridine-2,6-diamine ($H_3$pzpz) (1).** Di(6-amino-2-pyridyl)amine was synthesized according to the literature.[16]

A mixture of di(6-amino-2-pyridyl)amine (5.00 g, 24.8 mmol), chloropyrazine (6.84 g, 59.7 mmol), $Pd_2(dba)_3$ (0.46 g, 2 mol%), BINAP (0.62 g, 4 mol%) and Bu$^t$ONa (7.17 g, 74.6 mmol) in dry benzene (230 mL) was refluxed under argon with stirring for 4 days. Then the solvent was removed. The crude product was washed with water, benzene, and methanol and recrystallized from acetone (6.2 g, 70% yield). mp 282–283 °C; IR (KBr) $\nu/cm^{-1} = 3278$ w, 3202 w, 3117 w, 3058 w, 1618 m, 1594 m, 1586 m, 1551 s, 1526 s, 1508 m, 1448 vs, 1427 vs, 1376 w, 1361 w, 1345 w, 1311 m, 1270 w, 1248 m, 1155 m, 1006 m, 780 m, 772 m, 417 w; UV-Vis (DMF) $\lambda_{max}/nm$ ($\varepsilon/dm^3\ mol^{-1}\ cm^{-1}$) = 280 ($3.25 \times 10^4$), 347 ($2.98 \times 10^4$); MS(FAB): $m/z$ (%) 358 (10) $[M]^+$; $^1H$ NMR (400 MHz, $(CD_3)_2SO$): $\delta$ 9.75 (s, 2H), 9.40 (s, 1H), 9.26 (s, 2H), 8.22 (d, $J = 1.98$ Hz, 2H), 8.06–8.07 (d, $J = 3.42$ Hz, 2H), 7.53–7.59 (t, $J = 10.68$ Hz, 2H), 7.28–7.31 (d, $J = 10.68$ Hz, 2H), 7.08–7.11 (d, $J = 10.44$ Hz, 2H); EA (%) $C_{18}H_{15}N_9 \cdot 1/2CH_3COCH_3$: calcd. C 60.61, H 4.69, N 32.62; found: C 60.27, H 4.28, N 32.46.

***N*²-(pyrazin-2-yl)-*N*⁶-(6-(pyridin-2-ylamino)pyridin-2-yl)pyridine-2,6-diamine ($H_3$tpz) (2).** The reaction of *N*²-(6-bromopyridin-2-yl)-*N*⁶-(pyridin-2-yl)pyridine-2,6-diamine (5.0 g, 14.6 mmol) and aminopyrazine (1.67 g, 17.6 mmol) in the presence of $Pd_2(dba)_3$ (0.268 g, 2 mol%), BINAP (0.364 g, 4 mol%) and Bu$^t$ONa (2.39 g, 24.8 mmol) in dry benzene (200 mL) for 72 h gave a crude product of **2**. Then the solvent was removed. The crude product was washed with hot water, benzene, and recrystallized from acetone–methanol mixture. (3.8 g, 73% yield). mp 258–259 °C; IR (KBr) $\nu/cm^{-1} = 3262$ w, 3194 w, 3106 w, 3045 w, 1610 m, 1591 m, 1569 m, 1522 m, 1449 s, 1430 vs, 1348 w, 1327 w, 1306 s, 1240 m, 1201 m, 1152 m, 1074 w, 1051 w, 1008 w, 998 w, 838 w, 786 m, 738 w, 722 w; UV-Vis (DMF) $\lambda_{max}/nm$ ($\varepsilon/dm^3\ mol^{-1}\ cm^{-1}$) = 277 ($1.72 \times 10^4$), 350 ($1.75 \times 10^4$); MS(FAB): $m/z$ (%) 357 (20) $[M]^+$; $^1H$ NMR (400 MHz, $(CD_3)_2SO$): $\delta$ 9.75 (s, 2H), 9.40 (s, 1H), 9.26 (s, 2H), 8.22 (d, $J = 1.98$ Hz, 2H), 8.06–8.07 (d, $J = 3.42$ Hz, 2H), 7.53–7.59 (t, $J = 10.68$ Hz, 2H), 7.28–7.31 (d, $J = 10.68$ Hz, 2H), 7.08–7.11 (d, $J = 10.44$ Hz, 2H); EA (%) $C_{19}H_{16}N_8 \cdot 1/2CH_3OH$: calcd. C 62.89, H 4.87, N 30.09; found: C 63.14, H 4.50, N 29.90.

**$[Co_7(\mu_7\text{-pzpz})_4Cl_2]$ (3).** Anhydrous $CoCl_2$ (254 mg, 1.95 mmol), $H_3$pzpz (300 mg, 0.84 mmol) and naphthalene (65 g) were placed in an Ehrlenmeyer flask. The mixture was heated under argon and then a solution of potassium *tert*-butoxide (311 mg, 2.77 mmol) in *n*-butyl alcohol (5 mL) was added dropwise. The reaction was continued for another 12 h. The product was transferred to hexane for washing out naphthalene after being cooled, and then 100 mL *ca.* $CH_2Cl_2$ was used to extract the complex. A dark green complex was obtained after evaporation. The single crystals suitable for X-ray diffraction were obtained from diffusion of ether to a chloroform solution. (3.99 mg, 1% Yield), IR (KBr) $\nu$/cm$^{-1}$ = 3422 m, br, 1654 w, 1586 m, 1492 m, 1475 m, 1420 s, 1398 vs, 1349 s, 1338 s, 1262 w, 1157 s, 1032 w, 774 w, 668 w, 470 w; UV-Vis ($CH_2Cl_2$) $\lambda_{max}$/nm ($\varepsilon$/dm$^3$ mol$^{-1}$·cm$^{-1}$) = 231 (8.93 × 10$^4$), 279 (9.76 × 10$^4$), 385 (9.85 × 10$^4$), 594 (2.24 × 10$^4$), 647 (2.47 × 10$^4$); MS(FAB): *m*/*z* (%) 1901 (8) $[M]^+$, 1865 (9) $[M - Cl]^+$, 1357 (100) $[Co_5(Pzpz)_3]^+$; EA (%) $[Co_7(\mu_7\text{-pzpz})_4Cl_2]\cdot 2CHCl_3\cdot C_2H_5OC_2H_5$: calcd. C 42.32, H 2.73, N 22.78; found: C 42.22, H 2.44, N 22.90.

**$[Co_7(\mu_7\text{-pzpz})_4(NCS)_2]$ (4).** Solution of NaNCS (68 mg, 0.84 mmol) in $CH_3CN$ (2 mL) was added to a solution of **3** (38 mg, 0.02 mmol) in $CH_2Cl_2$ (50 mL). The mixture was stirred for 1 week, and then filtered. The filtrate was evaporated to dryness and gave a dark green compound, which was then purified by diffusion ether to the chloroform solution. The single crystals suitable for X-ray diffraction were obtained by slow evaporation of $CH_2Cl_2$–*n*-hexane solution. (33.8 mg, 87% Yield), IR (KBr) $\nu$/cm$^{-1}$ = 2057m, 1586 m, 1495 m, 1474 m, 1418 s, 1397 s, 1338 s, 1262 w, 1160 s, 1034m, 771w, 730 w; UV-Vis ($CH_2Cl_2$) $\lambda_{max}$/nm ($\varepsilon$/dm$^3$ mol$^{-1}$ cm$^{-1}$) = 231 (1.25 × 10$^5$), 278 (1.29 × 10$^5$), 391 (1.31 × 10$^5$), 595 (3.11 × 10$^4$), 631 (3.14 × 10$^4$); MS(FAB): *m*/*z* (%) 1946 (13) $[M]^+$, 1888 (10) $[M–NCS]^+$, 1357 (100) $[Co_5(pzpz)_3]^+$; EA (%) $[Co_7(\mu_7\text{-pzpz})_4(NCS)_2]\cdot CHCl_3\cdot C_2H_5OC_2H_5$: calcd. C 44.35, H 2.78, N 24.88; found: C 44.85, H 2.87, N 24.53.

**$[Co_7(\mu_7\text{-tpz})_4Cl_2]$ (5).** Compound **5** was synthesized using a procedure similar to that for **3**. (3.99 mg, 1% Yield), IR (KBr) $\nu$/cm$^{-1}$ = 1654 w, 1585 m, 1543 w, 1474 m, 1420 s, 1400 s, 1347 s, 1334 s, 1264 w, 1237 w, 1154 s, 1018 w, 963 w, 873 w, 814 w, 779 w, 729 w, 668 w; UV-Vis ($CH_2Cl_2$) $\lambda_{max}$/nm ($\varepsilon$/dm$^3$ mol$^{-1}$·cm$^{-1}$) = 232 (2.50 × 10$^4$), 287 (1.96 × 10$^4$), 396 (2.24 × 10$^4$), 587 (4.21 × 10$^3$), 638 (4.11 × 10$^3$), 854 (1.20 × 10$^3$); MS(FAB): *m*/*z* (%) 1898 (8) $[M]^+$, 1827 (9) $[M - 2Cl]^+$, 1355 (100) $[Co_5(tpz)_3]^+$; EA (%) $[Co_7(\mu_7\text{-tpz})_4Cl_2]\cdot 2CHCl_3\cdot C_2H_5OC_2H_5$: calcd. C 42.32, H 2.73, N 22.78; found: C 42.22, H 2.44, N 22.90.

**$[Co_7(\mu_7\text{-tpz})_4(NCS)_2]$ (6).** Compound **6** was synthesized using a procedure similar to that for **4**, and the single crystals suitable for X-ray diffraction were obtained from slow evaporation of ether to a $CH_2Cl_2$ solution. (33.0 mg, 85% Yield), IR (KBr) $\nu$/cm$^{-1}$ = 2064m, 1584 m, 1544 w, 1494 m, 1476 m, 1418 s, 1402 s, 1347 s, 1334 s, 1262 w, 1237 w, 1154 s, 1019 w, 964 w, 814 w, 765 w, 730 w, 668w; UV-Vis ($CH_2Cl_2$) $\lambda_{max}$/nm ($\varepsilon$/dm$^3$ mol$^{-1}$·cm$^{-1}$) = 231 (2.19 × 10$^4$), 284 (1.88 × 10$^4$), 395 (2.08 × 10$^4$), 584 (3.50 × 10$^2$), 626 (3.18 × 10$^3$), 857 (7.59 × 10$^2$); MS(FAB): *m*/*z* (%) 1943 (13) $[M]^+$, 1884 (10) $[M - NCS]^+$, 1826 (5) $[M - 2NCS]^+$, 1355 (100) $[Co_5(tpz)_3]^+$; EA (%) $[Co_7(\mu_7\text{-tpz})_4(NCS)_2]\cdot CHCl_3\cdot C_2H_5OC_2H_5$: calcd. C 46.68, H 2.97, N 22.30; found: C 46.58, H 3.17, N 22.61.

**Crystal structure determinations**

The chosen crystals were mounted on a glass fiber. Data collection was carried out on a NONIUS Kappa CCD diffractometer at 150(1) K using Mo-Kα radiation ($\lambda$ = 0.71073 Å) and a liquid nitrogen low-temperature controller. Cell parameters were retrieved and refined using the DENZO-SMN software on all reflections. Data reduction was performed on the DENZO-SMN software. Semi-empirical absorption was based on symmetry-equivalent reflections and absorption corrections were applied with the SORTAV program. All the structures were solved using SHELXS-97[17] and refined with SHELXL-97[18] by full-matrix least squares on $F^2$ values. The *R* factors are reasonable and accepted, in spite of the fact that they are higher than usual case because (a) the molecules are quite large and contain solvent molecules and (b) some atoms were found in disordered positions in every molecule.

For compound **4**, **5** and **6** there is a possible space-group ambiguity. We carefully examined structures of compounds **4**, **5** and **6**, and concluded that the *C*2/*c* and *P*2/*c* options are better than the *Cc* and *Pc* options for reasons which include:

(i) The intensities statistics show that both structures are super centric (mean $E^2$-1 is 1.178 for **4**, 1.328 for **5**, and 1.301 for **6** where 0.968 is expected for centrosym and 0.736 for non-centrosym.)

(ii) We solved structures of **4** and **6** in the *C*2/*c* and *Cc* options, and **5** in the *P*2/*c* and *Pc* options, and checked with PLATON check-CIF. The reports of *C*2/*c* and *P*2/*c* options only gave several alerts in level C, but the reports of *Cc* and *Pc* options gave alerts in level A & B (detection of centre of symmetry and many others).

(iii) The dimensions of the *C*2/*c* and *P*2/*c* options are more meaningful than the *Cc* and *Pc* options.

CCDC reference numbers 623294–623297.

For crystallographic data in CIF or other electronic format see DOI: 10.1039/b614661a

## Acknowledgements

The authors acknowledge financial supports from the National Science Council and the Ministry of Education of the Republic of China. We are also grateful to Mr Shih-Chi Wang for his helps with magnetic measurement.

## References

1 (*a*) S.-Y. Lin, I.-W. P. Chen, C.-H. Chen, M.-H. Hsieh, C.-Y. Yeh, T.-W. Lin, Y.-H. Chen and S.-M. Peng, *J. Phys. Chem. B*, 2004, **108**, 959; (*b*) J. F. Berry, F. A. Cotton, L. M. Daniels and C. A. Murillo, *J. Am. Chem. Soc.*, 2002, **124**, 3212; (*c*) I.-W. P. Chen, M.-D. Fu, W.-H. Tseng, J.-Y. Yu, S.-H. Wu, C.-J. Ku, C.-H. Chen and S.-M. Peng, *Angew. Chem., Int. Ed. Engl.*, 2006, 5414.

2 (*a*) E.-C. Yang, M.-C. Cheng, M.-S. Tsai and S.-M. Peng, *J. Chem. Soc., Chem. Commun.*, 1994, 2377; (*b*) S.-J. Shieh, C.-C. Lin, I. Chao, C.-C. Wang and S.-M. Peng, *Chem. Commun.*, 1996, 315; (*c*) C.-K. Kuo, J.-C. Chang, C.-Y. Yeh, G.-H. Lee, C.-C. Wang and S.-M. Peng, *Dalton Trans.*, 2005, 3696; (*d*) R. Clérac, F. A. Cotton, L. M. Daniels, K. R. Dunbar, K. Kirschbaum, C. A. Murillo, A. A. Pinkerton, A. J. Schutz and X. Wang, *J. Am. Chem. Soc.*, 2000, **122**, 6226; (*e*) J. F. Berry, F. A. Cotton, T. Lu, C. A. Murillo, B. K. Roberts and X. Wang, *J. Am. Chem. Soc.*, 2004, **126**, 7082; (*f*) J. F. Berry, F. A. Cotton and C. A. Murillo, *Dalton Trans.*, 2003, 3015; (*g*) J. F. Berry, F. A. Cotton, L. M. Daniels, C. A. Murillo and X. Wang, *Inorg. Chem.*, 2003, **42**, 2418.

3 S.-Y. Lai, T.-W. Lin, Y.-H. Chen, C.-C. Wang, G.-H. Lee, M.-H. Yang, M.-K. Leung and S.-M. Peng, *J. Am. Chem. Soc.*, 1999, **121**, 250.

 

4 (*a*) C.-Y. Yeh, Y.-L. Chiang, G.-H. Lee and S.-M. Peng, *Inorg. Chem.*, 2002, **41**, 4096; (*b*) S.-J. Shieh, C.-C. Chou, G.-H. Lee, C.-C. Wang and S.-M. Peng, *Angew. Chem., Int. Ed. Engl.*, 1997, **36**, 56; (*c*) C. Y. Yeh, C. H. Chou, K. C. Pan, C. C. Wang, G. H. Lee, Y. O. Su and S. M. Peng, *J. Chem. Soc., Dalton Trans.*, 2002, 2670; (*d*) C.-C. Wang, W.-C. Lo, C.-C. Chou, G.-H. Lee, J.-M. Chen and S.-M. Peng, *Inorg. Chem.*, 1998, **37**, 4059; (*e*) J. F. Berry, F. A. Cotton, P. Lei, T. Lu and C. A. Murillo, *Inorg. Chem.*, 2003, **42**, 3534.
5 (*a*) C.-H. Chien, J.-C. Chang, C.-Y. Yeh, G.-H. Lee, J.-M. Fang and S.-M. Peng, *Dalton Trans.*, 2006, 2106; (*b*) C.-H. Chien, G.-H. Lee, Y. Song and S.-M. Peng, *Dalton Trans.*, 2006, 3249.
6 (*a*) S.-Y. Lai, C.-C. Wang, Y.-H. Chen, C.-C. Lee, Y.-H. Liu and S.-M. Peng, *J. Chin. Chem. Soc.*, 1999, **46**, 477; (*b*) Y.-H. Chen, C.-C. Lee, C.-C. Wang, G.-H. Lee, S.-Y. Lai and S.-M. Peng, *Chem. Commun.*, 1999, 1667.
7 (*a*) S.-M. Peng, C.-C. Wang, Y.-L. Jang, Y.-H. Chen, F.-Y. Li, C.-Y. Mou and M.-K. Leung, *J. Magn. Magn. Mater.*, 2000, **209**, 83; (*b*) R. H. Ismayilov, W.-Z. Wang, R.-R. Wang, C.-Y. Yeh, G.-H. Lee and S.-M. Peng, *Chem. Commun.*, 2006, 10.1039/b614597c.
8 C. K. Kuo, G.-H. Lee and S.-M. Peng, unpublished work from our group.
9 R. H. Ismayilov, W.-Z. Wang, G.-H. Lee and S.-M. Peng, *Dalton Trans.*, 2006, 478.
10 R. H. Ismayilov, W.-Z. Wang, G.-H. Lee, R.-R. Wang, I. P.-H. Liu, C.-Y. Yeh and S.-M. Peng, unpublished work from our group.
11 C.-Y. Yeh, C.-C. Wang, Y.-H. Chen and S.-M. Peng, in *Redox Systems Under Nano-Space Control*, ed. T. Hirao, Springer, Germany, 2006, ch. 5.
12 D. A. Pantazis and J. E. McGrady, *J. Am. Chem. Soc.*, 2006, **128**, 4128.
13 S. Kermer, W. Henke and D. Reinen, *Inorg. Chem.*, 2003, **42**, 3534.
14 (*a*) P. Kiehl, M.-M. Rohmer and M. Benard, M, *Inorg. Chem.*, 1982, **21**, 3013; (*b*) D. L. Williams, D. W. Smith and R. C. Stoufer, *Inorg. Chem.*, 1967, **6**, 590.
15 (*a*) C. Mealli and D. M. Proserpio, *J. Chem. Educ.*, 1990, **67**, 399; (*b*) P. Angaridis, In *Multiple Bonds Between Metal Atoms*, 3rd edn, ed. F. A. Cotton, C. A. Murillo and R. A. Walton, Springer Science and Business Media, Inc., New York, 2005; (*c*) P. Kiehl, M.-M. Rohmer and M. Bénard, *Inorg. Chem.*, 2004, **43**, 3153.
16 J. Bernstein, B. Stearns, M. Dexter and W. A. Lott, *J. Am. Chem. Soc.*, 1947, **69**, 1147.
17 G. M. Sheldrick, *SHELXS-97, Program for solution of crystal structures*, University of Göttingen, Germany, 1997.
18 G. M. Sheldrick, *SHELXL-97, Program for refinement of crystal structures*, University of Göttingen, Germany, 1997.